Supporting Information

Waldauer et al. 10.1073/pnas.1005415107

SI Text

Serpentine Mixer Properties. The serpentine mixer used in these experiments was first described by Hoffman et al. (1) and in detail by Kane et al. (2) and is shown in Fig. S1. Sample and diluent are combined in a T-region and mixed using a chaotic advection mechanism (Dean and corner vortices as described by Chamarthy and Wereley) (3) composed of a 5 turn serpentine region. Following the mixing region the chip has two observation regions, the first 120 μm wide for measurements on a fast time scale and the second 1,000 μm wide for measurements on a timescale an order of magnitude larger (the wider region was not used in the protein L experiments).

Mixing Efficiency. Confocal imagery of cross-sections of microfluidic channel following mixing can be used to characterize the mixing efficiency according to the equation (3):

$$\mathrm{CoV} = \frac{\sigma}{I_m} = \frac{\sqrt{\frac{\sum_i^N (I_i - I_m)^2}{N-1}}}{I_m}$$

where I is the intensity at a given pixel and I_m is the mean intensity. When used on the cross-sectional images shown in Fig. S2, the top image (A) where the total flow rate is too low for chaotic advection, the CoV value is 1.64. For the flooded instance shown in the bottom image (C), the CoV is much lower with a value of 0.17. For perfect mixing, image would be uniform within the channels and have a CoV of exactly 0. The middle image shows efficient mixing and has a CoV of 0.15, which is very comparable to that of the flooded instance. As shown in Fig. S3, which plots the CoV as a function of Reynolds number, that Re = 60 or higher produce efficient mixing.

Serpentine Mixer Fabrication. The microfluidic mixer chip is fabricated from a highly polished UV grade 500 μm thick fused silica substrate (SENSOR Prep Services). Features are transferred to the wafers through standard photolithography and are etched into the substrate through a highly selective oxide etcher (NLD570 Oxide Etcher, ULVAC Technologies). Through-ports are drilled through the substrate using a tabletop computer controlled mill equipped with a diamond bit (WOLFCO). Lastly, the devices are sealed with a 170 μm thick wafer with identical properties to that of the substrate through a direct bonding procedure.

Sources of Uncertainty of Measurement. Determination of time after mixing depends on knowing the position of the probe beam within the mixer. Prior to contact quenching measurements, the chip is filled with 10 mM Fluorescein and the optical absorbance at 442 nm is recorded as the chip is scanned in two dimensions to locate the exact position of the mixing-region observation-region interface, which is used to define t_0. The step size of this scan is 20 μm. For measurements taken inside the 120 μm wide observation channel, uncertainty in time for any measurement is the sum of the uncertainties from the identification of t_0 (±20 μm). The uncertainty of individual positions relative to t_0 is due to the resolution of the optically encoded translation stage is ±80 nm, which is negligible in comparison with other uncertainties. The uncertainty of the location of the pump beam within the probe beam diameter is estimated to be 5% of the probe beam, ∼5 μm. The total error in distance is therefore 20.6 μm. Since all distances are at least 550 μm from t_0, this error is no more than 3.7%.

The linear flow velocity is determined by the syringe pump flow rate and the cross-sectional area of the exit channel with the largest error arising from the uncertainty in the depth of the etched channel (±5% of the measured depth, ∼2 μm). A further systematic error is the parabolic flow profile across the depth of the chip. The triplet absorption measurement can probe a molecule anywhere within the 40 μm-deep channel. For a flow rate of 1 m/s in the center, the standard deviation of flow rates is 0.37 m/s. This is commensurate with the observed exponential lifetime (∼50 μs) of long-lived photoproducts in the beam diameter (∼50 μm). This spread in the flow rate is therefore always the dominant uncertainty and all measured times in Fig. 1*C* have an uncertainty of 37% along the x-axis and can account for the entire scatter in the plot. Note that this uncertainty does not affect the measured intramolecular contact rates, such as that in Fig. 1*B*, as they are about 10 times faster than the flow rate through the probe beam.

Determination of *D* Using SSS Theory. The reaction-limited and diffusion-limited rates can be expressed as (4)

$$k_R = \int_a^\infty q(r)P(r)dr$$

$$\frac{1}{k_{D+}} = \frac{1}{k_R^2 D}\int_a^{l_c} \frac{dr}{P(r)}\left\{\int_r^{l_c}(q(x) - k_R)P(x)dx\right\}^2$$

where r is the distance between the tryptophan and cysteine and $P(r)$ is the probability density of finding the polypeptide at that distance. D is the effective intramolecular diffusion coefficient, a is the distance of closest approach (typically defined to be 4 Å), l_c is the contour length of the peptide and $q(r)$ is the distance-dependent quenching rate. The distance-dependent quenching rate for the Trp-Cys system has been determined experimentally (5) and drops off exponentially beyond 4 Å, so the reaction-limited rate is mostly determined by the probability of the shortest distances. Thus the only free parameters in the equations above are D and $P(r)$.

Singh et al. used a worm-like chain with excluded volume to model the equilibrium measurements of k_R in protein L and then used the $P(r)$ that best fit the measured rates to determine D using the measured k_{D+}. This analysis revealed ∼6 fold decrease in D between 6 M and 2.3 M GdnHCl (6), but below 2 M GdnHCl, $k_R \gg k_{D+}$ and cannot be resolved experimentally so the parameters of the model cannot be calibrated to low denaturant. Hoffman et al. modeled single molecule measurements of intramolecular FRET with a Gaussian distribution in which $\langle r^2 \rangle = 2l_p l_c$, where l_c is the contour length between the probes (ie, W47 and C57) and l_p is the persistence length determined experimentally in various concentrations of denaturant as low as 0.6 M GdnHCl (7). It is unlikely that a simple Gaussian or worm-like chain model would accurately describe an unfolded protein in low denaturant since such a model does not account for any attractive interactions that would be physically realistic in water. Therefore k_R is too low and the calculated D is probably an upper limit. Alternatively, we can consider a recent set of molecular dynamics (MD) simulations of protein L in implicit solvent which determined $P(r)$ at various temperatures between 300 and 450 K (8). This study found a correspondence between simulated distributions at elevated temperatures and measurements of k_R in various concentrations of denaturant which could be calibrated

with a coil-globule model. However, the MD distributions are probably more compact than is realistic since implicit solvent simulations tend to overly stabilize compact states (8). This would lead to larger k_R and therefore represent a lower limit on D. Table S1 shows the parameters of these two models and the calculated diffusion coefficients.

1. Hoffmann A et al. (2007) Mapping protein collapse with single-molecule fluorescence and kinetic synchrotron radiation circular dichroism spectroscopy. *Proc Natl Acad Sci USA* 104(1):105–110.
2. Kane AS et al. (2008) Microfluidic mixers for the investigation of rapid protein folding kinetics using synchrotron radiation circular dichroism spectroscopy. *Anal Chem* 80(24):9534–9541.
3. Chamarthy P, Wereley S (2004) Mixing characteristics in a serpentine micro-channel. *Proceedings of the IMECE'04*.
4. Lapidus LJ, Steinbach PJ, Eaton WA, Szabo A, Hofrichter J (2002) Effects of chain stiffness on the dynamics of loop formation in polypeptides. Appendix: Testing a 1-dimensional diffusion model for peptide dynamics. *J Phys Chem B* 106(44):11628–11640.
5. Lapidus LJ, Eaton WA, Hofrichter J (2001) Dynamics of intramolecular contact formation in polypeptides: Distance dependence of quenching rates in a room-temperature glass. *Phys Rev Lett* 87(25).
6. Singh VR, Kopka M, Chen Y, Wedemeyer WJ, Lapidus LJ (2007) Dynamic similarity of the unfolded states of proteins L and G. *Biochemistry* 46:10046–10054.
7. Hoffmann A et al. (2007) Mapping protein collapse with single-molecule fluorescence and kinetic synchrotron radiation circular dichroism spectroscopy. *Proc Natl Acad Sci USA* 104(1):105–110.
8. Voelz VA, Singh VR, Wedemeyer WJ, Lapidus LJ, Pande VS (2010) Unfolded-state dynamics and structure of protein L characterized by simulation and experiment. *J Am Chem Soc* 132(13):4702–4709.

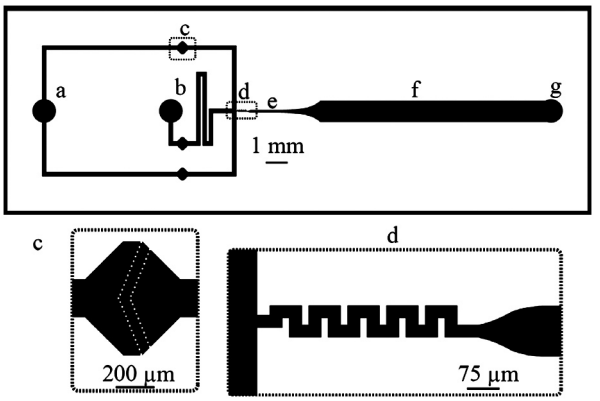

Fig. S1. Geometry of the chaotic advection mixing microfluidic-chip. (*A*) Buffer inlet. (*B*) Protein solution inlet. (*C*) Filter section (one of three total per chip). Each filter post is a 10 by 10 µm square and they are spaced 10 µm apart. (*D*). The serpentine mixing region is composed of five turns and the channel is 30 µm wide. (*E*) The narrow observation region is 120 µm wide and 1.4 mm long. (*F*) The wide observation region is 1000 µm wide and 10.4 mm long. (*G*) Outlet port.

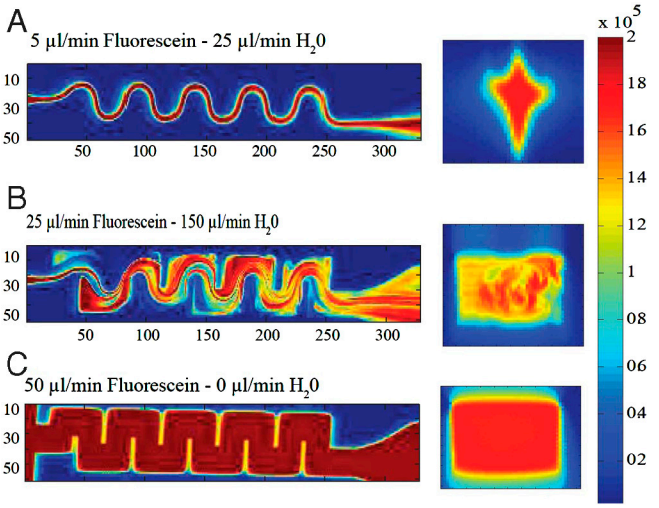

Fig. S2. Confocal microscopy images taken of the serpentine mixer at different flow rates, in plane with the serpentine on left and cross section of the channel immediately following the serpentine at right. (*A*) Image showing no mixing because the Reynolds number is too low (Re = 14.3). Note that a jet of the Fluorescein solution produced by the *T* at the start of the mixer progresses through the serpentine without any interference. (*B*) The effects of Dean and corner vortices can be seen here at flow with Re = 83. (*C*) Image of the full channel is shown by flowing only Fluorescein solution. Mixing is also evident from the cross-sectional image (right panels).

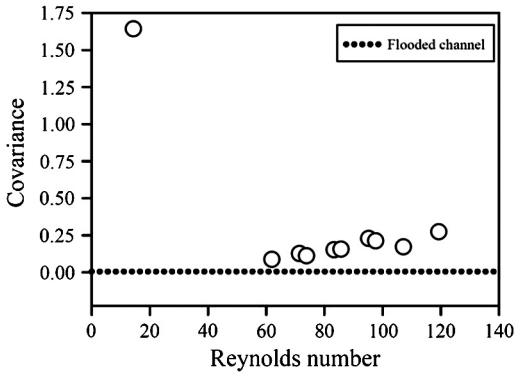

Fig. S3. Plot showing mixing efficiency, as defined by equation 1 as a function of Reynolds number. Flow with very low Reynolds number, Re = 14 produces a very high covariance, however at Re ≥ 60, the covariance is much closer to that of the flooded channel.

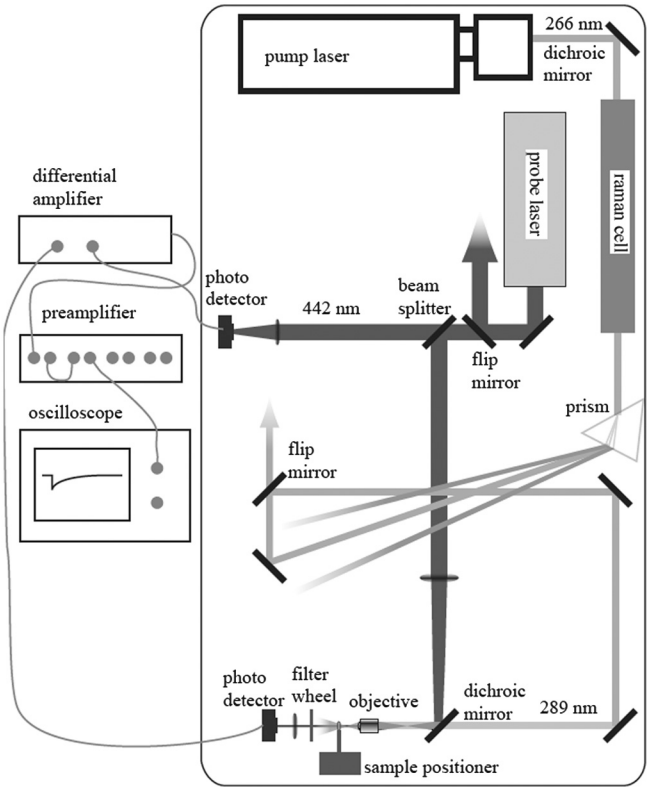

Fig. S4. Schematic of tryptophan triplet instrument coupled to serpentine mixing chip.

Table S1. Determination of diffusion coefficients from measured data using two models

			$P(r)$ from MD (8)		$P(r)$ from Gaussian (7)		
[GdnHCl] (M)	$k_{obs} \sim k_{D+}$ (s^{-1})	T (K)	k_R (s^{-1})	D ($cm^2\ s^{-1}$)	l_p (Å)	k_R (s^{-1})	D ($cm^2\ s^{-1}$)
0.2	1.05×10^5	300	3.4×10^7	6.5×10^{-10}	4.0	1.6×10^7	2.5×10^{-9}
0.7	1.31×10^5	330	4.1×10^7	9.3×10^{-10}	5.0	1.2×10^7	4.6×10^{-9}
1.1	1.53×10^5	370	3.3×10^7	1.1×10^{-9}	6.2	8.6×10^6	7.5×10^{-9}